NUMERICAL 3D RANS SIMULATION OF GAS-LIQUID FLOW IN A CENTRIFUGAL PUMP WITH AN EULER-EULER TWO-PHASE MODEL AND A DISPERSED PHASE DISTRIBUTION

T. Müller - P. Limbach - R. Skoda

Ruhr-Universität Bochum, Chair of Hydraulic Fluid Machinery (HSM),
Universitätsstraße 150, 44801 Bochum, Germany, tim.mueller-g6g@ruhr-uni-bochum.de

ABSTRACT

A numerical study is performed in order to evaluate the capability of the mono-dispersed multiphase model in ANSYS CFX to predict the flow of liquid-gas mixture in radial pumps. A radial research pump with annulus casing and low rotational speed is investigated for different operation points. The drag force is approximated by the Schiller Nauman model. No other interfacial forces are considered. Both, liquid and gaseous phase are treated incompressible. The inlet gas volume fraction is varied up to 7 %. The comparison of a full-geometry model and a single blade model shows that the single blade model predicts the head sufficiently accurate. A grid study is performed for single-phase flow. Head as well as blade pressure profiles are compared to experimental data. For IGVF up to 3 % the head is predicted with a good accuracy. While the experimental blade pressure profiles indicate that the accumulation of gas is located close to the blade surface, the simulation predicts their location rather in the channel center. This mislocation of large gas zones leads to an even qualitatively wrong head drop in the simulation for IGVF > 3 % and high flow rates. It can be concluded that the accuracy of the multiphase model needs to be improved, particularly by the consideration of lift force and bubble interaction, for a reliable simulation of liquid-gas flow in radial pumps, in particular at higher IGVF.

NOMENCLATURE

Roman symbols

b	Width	[m]
c_D	Dimensionless drag coefficient	[−]
d	Diameter	[m]
g	Gravitational force	[m s^{-2}]
H	Pump head	[m]
M_k	Interfacial forces	[kg m^{-3} s^{-1}]
n	Rotational speed	[s^{-1}]
n_q	Specific speed	[s^{-1}]
p	Pressure	[Pa]
Q	Flow rate	[m^3 s^{-1}]
Re	Reynolds number	[−]
s	Blade thickness	[m]
T	Timestep	[°]
u	Velocity	[m s^{-1}]
z	Number of blades	[−]

Abbreviations

CFD	Computational fluid dynamics
GVF	Gas volume fraction
IGVF	Inlet gas volume fraction

Greek Charackters

α	Gas volume fraction	[−]
β	Blade angle	[°]
η_i	Inner efficiency	[%]
μ	Dynamic viscosity	[m^2 s^{-1}]
ρ	Density	[kg m^{-3}]

Subscripts

1,2	Impeller position 1 and 2	
B	Bubble	
g	Gaseous	
k	Phase	
l	Liquid	
opt	Best efficiency flow rate	
s	Static	
swg	Side wall gap	
t	Total	
tot	Total at inlet	

MP	Monitor point	
MPP$_i$	Monitor point pressure at radial position i	
MPS	Monitor point suction	

INTRODUCTION

Usually, radial centrifugal pumps (low specific speed) are designed for pure liquids. For the transport of liquid-gas mixtures, even at very low values of the IGVF of 1 % or 2 % the head may drop, usually more significant in part and overload (low and high flow rates) operation conditions than for nominal flow rate. As a source of the head drop, phase separation and large gas accumulations within the blade channel due to the Coriolis force, the slip between bubbles and liquid as well as pressure gradients in cross-flow direction have been identified (Sato et al. 1996). In axial pumps a secondary flow reduces the tendency of phase separation, so that axial pumps can handle higher gas volume fractions than radial ones (Gülich, 2010). The present paper focuses on the flow in radial pumps. Previous experimental studies of the two-phase flow characteristics of radial pumps have shown a decrease of head even at low gas loading (Cappelino et al., 1992, Furukawa et al., 1988, Murakami et al., 1971, Tillack, 1998). A significant decrease of head in part- and overload occurs, whereas at design point the pump is able to handle higher IGVF (Cappelino et al., 1992). Murakami et al. (1971) have experimentally carried out that a radial pump can be operated at higher IGVF if the rotational speed is increased, since the air bubbles crash into finer bubbles. The motion of air bubbles has been theoretically analyzed for a radial pump by Minemura and Murakami (1980). They have solved the equation of motion for air bubbles in the flow field including the effects of the drag force and slip, density differences between the phases and inertia force. By comparing their results to the experimental data, they have demonstrated that the bubble motion within the impeller is controlled by the corresponding drag force and the pressure gradient around the bubble. The tendency that bubbles deviate from the streamlines of liquid water raises with increasing bubble diameter. Numerical simulations of the flow in radial pumps have been carried out by Minemura and Uchiyama (1993a). For low IGVF small deviations have been found between simulation and experimental data. However, at high IGVF the head drop is underestimated in the simulation. Significant deviations have also been found for the numerical investigation of a high specific speed pump (Caridad et al., 2008, Yu et al., 2012). A numerical study of the region of bubble accumulation in a radial pump has been performed by Minemura and Uchiyama (1993b) as well as Pak and Lee (1998). Both have carried out that the bubbles move to the shroud of the impeller as well as to the suction surface of the blade and assume that the head drop is a result of the gas accumulation.

The previous attempts of numerical simulation of the liquid-gas mixture in radial pumps have in common, that they show significant deviations between predicted and experimentally determined head drop, especially for higher values of IGVF. Therefore, the aim of this paper is the assessment of a common simulation method (ANSYS CFX) to predict the pump head of a radial pump ($n_q = 32$ min^{-1}) at design and off-design conditions for IGVF of 1 % to 7 %. A mono dispersed phase distribution and a constant bubble diameter size is assumed. Bubble population, breakup, and coalescence as well as lift force are neglected. Global performance parameters of the pump such as pressure head, power consumption and pump efficiency for single-phase flow (water) and pump head as well as blade pressure for two-phase flow (gas/water) are determined, and validated against existing experimental data.

METHODOLOGY

Pump characteristics

Experimental data, i.e. performance data as well as blade pressure profiles by Suryawijaya and Kosyna (2000) and Wulff (2014) on a radial research pump is used for validation. The pump design is optimized for flow visualization within the impeller as well as blade pressure measurements. Flow visualizations as described by Wunderlich (1981) and performed in a scaled-down (scale 1:0.5) variant of the research pump, indicate that there is a highly unsteady flow field, and that gas accumulates at different location at the blade surfaces, Wunderlich (2014).
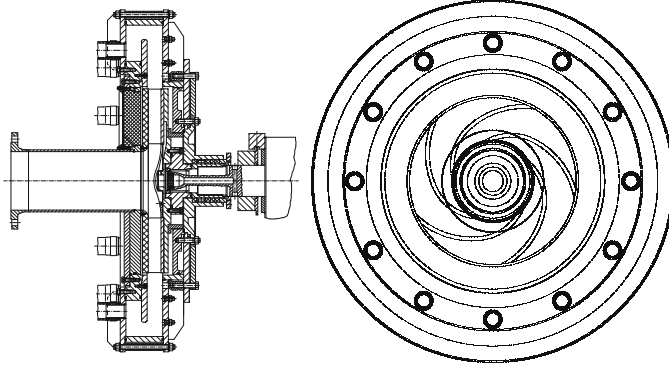
Figure 1: **Cross section of the centrifugal pump**

Table 1: **Pump geometry data**

Impeller inlet diameter	d_1	260 mm
Blade inlet width	b_1	46 mm
Impeller blade inlet angle	β_1	19°
Impeller outlet diameter	d_2	556 mm
Blade outlet width	b_2	46 mm
Impeller blade outlet angle	β_2	23°
Blade thickness	s	13 mm
Blade shape		2 circular arc
blade number	z	5

The pump is characterized by a closed impeller with a simple blade design based on two circular arcs and a low rotational speed. A rotation-symmetrical annulus instead of a volute chamber is used to obtain essentially uniform flow conditions downstream of the impeller and to simplify the numerical modeling. Geometry details of the pump are listed in table 1 and the pump performance data in table 2.

Table 2: **Pump performance data**

		SI units	industry units
Nominal flow rate	Q_{opt}	$0.114\ m^3/s$	$412\ m^3/h$
Nominal pump head	H_{opt}	$10.16\ m$	$10.16\ m$
Nominal rotational speed	n_{opt}	$9\ s^{-1}$	$540\ min^{-1}$
Specific speed	n_q	$0.535\ s^{-1}$	$32\ min^{-1}$

Due to the specific design the head characteristics has a rather flat slope and the efficiency does not decrease significantly towards overload, cf. fig. 4. In fact, a significant recirculation within the impeller is present even at nominal flow rate so that the presence of a distinct best efficiency point is not discernible.

Numerical method and two-phase model

The commercial 3D RANS CFD-solver ANSYS CFX version 15 is used for the flow simulation of water-air mixtures. The momentum equation and continuity equation are solved in a coupled way. Since the coupled solution of momentum equation and continuity equation together with the volume fraction equation shows a poor residuum, the volume fraction equation is solved in a segregated way, i.e. decoupled from momentum and continuity equation. This approach shows a better residuum drop. Double-precision accuracy of floating point numbers and second discretization order in space and time is chosen, assuming a mono-dispersed phase distribution and a constant diameter size of perfectly spherical bubbles. The Eulerian description of the dispersed phase is preferred to the Lagrange approach, since it is assumed that Euler-methods have better numerical properties regarding grid dependency (Wan and Peters, 1999) and their validity in regions where the dispersed phase is dense, i.e. very high gas volume fractions (GVF). High GVF are in fact present in regions with gas accumulation in the blade channels, as it is demonstrated in the result section. The good performance of Euler methods for liquid-gas mixtures is confirmed by the simulations of bubble columns (Hlawitschka et al., 2011, Krepper et al. 2007).

It is essential to solve two different velocity fields (inhomogeneous flow), one for each phase, to allow phase separation of air and water. The turbulence fields are also treated in a non-homogeneous

3

way. The pressure field is modelled in a homogenous way, i.e. shared by all fluids. The conservation equations of mass and momentum for unsteady turbulent flow of multiple phases k ($k = l,g$) can be written as follows:

$$\frac{\partial}{\partial t}(\alpha_k \rho_k) + \nabla \cdot (\alpha_k \rho_k u_k) = 0 \tag{1}$$

$$\frac{\partial}{\partial t}(\alpha_k \rho_k u_k) + \nabla \cdot (\alpha_k \rho_k u_k u_k) = -\alpha_k \nabla p + \nabla \cdot (\alpha_k \mu_k (\nabla u_k + (\nabla u_k)^T)) + M_k \tag{2}$$

The lift forces are neglected, since to the knowledge of the authors, no validated lift model is available for the specific flow conditions in radial pumps, i.e. separated turbulent flow and strong pressure gradients due to Coriolis and centrifugal forces. All other interfacial forces but drag forces are neglected, too. The drag force acting on the liquid phase l can be written as follows:

$$M_l = -M_g = \frac{3}{4} c_D \frac{\rho_l}{d_B} \alpha_g \left| u_g - u_l \right| \tag{3}$$

The dimensionless drag coefficient c_D is calculated by the Schiller Naumann drag law (Schiller and Nauman, 1933, ANSYS Inc., 2014), cf. equation 4.

$$c_D = max(\frac{24}{Re}(1 + 0.15 Re^{0.687}), 0.44) \tag{4}$$

Preliminary tests have shown that an incompressible treatment of the gas phase enhances the stability of the CFD solver significantly and hardly changes the results, so that both phase are treated incompressible.

Set-up

Two geometrical models have been set-up, a full geometry and a single blade channel model, cf. fig. 2 for a schematic meridian view of both models. Regarding the single channel model, due to the simple geometry of the annulus chamber, the same flow field in each blade channel is assumed. Since the impeller has 5 blades the model consists of a 72° segment and periodic boundary conditions in circumferential direction. The annulus chamber has been simplified by a radial outflow surface. A confuser is added at the radial outlet flow section because it avoids flow separation due to the adverse pressure gradient in the annulus and therefore stabilizes the numerical flow solver. The confuser reduces the radial outflow surface to 60 % of the radial outflow surface of the impeller. In the single channel model, the side chambers are neglected. To avoid influence of a too close inlet boundary on the prediction of the part load swirl the axial length of the suction pipe is extended to three times the diameter of the pipe.
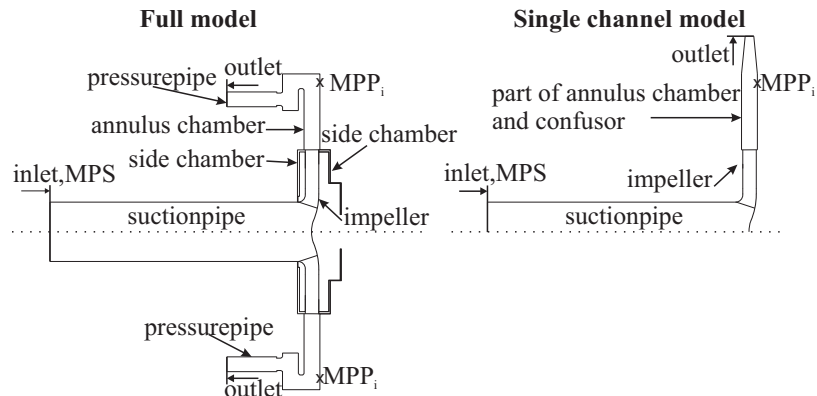

Figure 2: **Schematic meridian view of the numerical models**

For verification of the single channel model, a full geometry model is investigated, containing the impeller, the annulus chamber, the side chambers as well as the suction pipe and the pressure pipes – there are 12 pressure pipes mounted at the annulus, uniformly distributed in circumferential direction. The subsequent evaluation of the impeller outlet pressure and the head is done on the same radial positions for the full and single channel model, indicated as MPPi in fig. 2., i = 1 to 8.

The numerical set-up is summarized in table 3. For the full model, steady simulations for 3 different rotational speeds and about 8 operation points per speed have been performed on a grid with about 1.1 million nodes. For the single channel model, steady simulations only for $n = 540\ 1/min$ have been performed. The governing equations in the impeller are solved in the relative motion frame. All single-phase flow simulations with the single channel model fulfill the convergence criteria. However, for about 60 % of the full model single-phase simulations the residua do not drop below the criterion of $1.e^{-4}$. There is no particular operation range, where these convergence difficulties occur. Since transient simulations are very costly and it can be assumed that integral values as the pump head are assessable even though the residua have not dropped by the full 4 orders of magnitude in steady simulations, an approximative convergence criterion has been applied. For a sufficiently long time interval, where the residua do not decrease further but oscillate around an average level, it can be observed that the standard deviation of the head and the inner power are significantly lower than 1 % of the average. Therefore, this average can be assumed to be a suitable estimation of the final value. In order to verify this approximative convergence criterion for steady state results, exemplary transient simulations are performed (absolute frame of reference, i.e. moving rotor and a sliding interface between impeller and static components) for the full model and two operation points ($n = 540\ 1/min$, flow rates 350 m^3/h and 412 m^3/h) with particular poor steady state convergence behavior and with a time step size that corresponds to $1°$ rotational of the impeller. After a number of about 25 revolutions the head and inner power have approached steady state values. The time average over the last complete impeller revolution shows a deviation of less than 0.5 % percent to the results of the steady simulations, so that it can be concluded that the much less time consuming steady simulation is accurate enough for the evaluation of the performance curves.

Table 3: **CFD setup**

	Single-phase flow	**Two-phase flow**
Fluid	Water ($\rho_l = 998\ kg/m^3$)	Water ($\rho_l = 998\ kg/m^3$), air ($\rho_g = 1.185\ kg/m^3$, $d_B = 0.5\ mm$)
Morphology	Continuous phase	Continuous (water) and dispersed phase (air)
Turbulence model	Shear stress transport	Shear stress transport
Inlet boundary	Mass flow water	Mass flow water and air, IGVF
Outlet boundary	Static pressure	Static pressure
Wall boundary	Adiabatic, smooth, non-slip condition	Adiabatic, smooth, non-slip condition
Rotation treatment	steady (relative frame)	transient (relative frame)
Convergence criteria	Max residuals < $1.e^{-4}$, imbalances < 1 %, stability of macro (head, torque) and local (pressure, velocity) parameters < 1 %	Max residuals < $1.e^{-3}$, imbalances < 1 %,

The computational grids are generated by the commercial packages ICEM and TURBOGRID. For the full model and single-phase flow, the results are compared on a coarse (1.1 million nodes, average y+ = 80) and a fine (4 million nodes, average y+ = 18) mesh. Since a poor grid quality does

not allow the residua to drop significantly, the drop of the residua by at least 4 orders of magnitude for a couple of operation points is an indication for a sufficiently good grid quality. The results of the grid study are shown in figure 4, where the head H, the inner power P_i and the inner efficiency η_i are compared for both grids and the data for a rotational speed of $n = 540 \ 1/min$. The maximum deviation of the head between both grids occurs at the nominal flow rate and equals 1.4 %. For the inner power the deviation is even below 0.5 %. In addition the maximum deviation of local parameters (pressure, velocity) at different MP between both grids is 0.5 %. Therefore, it can be concluded that this deviation is small enough, so that all subsequently discussed results are obtained by the coarse grid. The corresponding coarse single channel grid has a node number of about 66 thousand.
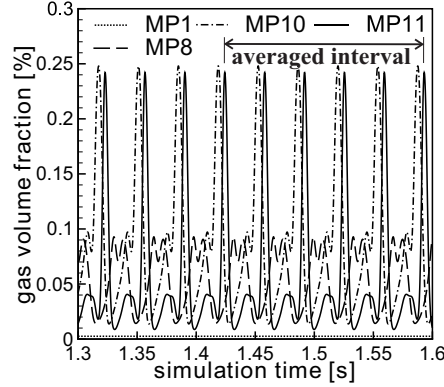
Figure 3: **Periodicity interval**

All two-phase flow simulations have been performed on the single channel model assuming that the findings of the single-phase flow grid study are transferable on the two-phase flow, an assumption which is a first starting point for such investigations and which is to be verified in the future. Due to the bubble diameter has not been measured in the experiment, a constant bubble diameter size of $0.5 \ mm$ is assumed, according to the measurement by Minemura et al. (1985). Since steady state results could not be obtained due to the highly-unsteady nature of the flow, all simulations have been done in a transient way within the relative frame of motion, i.e. with frozen rotor. The time step size corresponds to $0.5°$ rotation angle, and the maximum residuum of all equations drop by at least 3 orders of magnitude. The gas volume fraction is monitored in the course of time at different MP within the blade channel and shows two types of simulation results. One type with a stationary behavior of the GVF and the other with an oscillation behavior. The results of the type with an oscillation behavior are time averaged for a sufficiently long time interval of 5 periods (cf. figure 3).

RESULTS

Evaluation of integral values

The evaluation of the integral values in the simulation follows the same procedure as in the experiment. The pump head is calculated by equation (5). The total pressure difference between eight circumferentially with equal spacing arranged monitor points (p_{t,MPP_i}, cf. Figure 2), which are located at a constant radius in the annulus chamber, and the total inlet pressure ($p_{t,MPS}$, cf. Figure 2.) is determined.

$$H = \frac{\dfrac{\sum\limits_{i=1}^{8} p_{t,MPP_i}}{8} - p_{t,MPS}}{g\rho_l} \tag{5}$$

For two-phase flow simulations the pump head is evaluated by equation (6). In that case the density of water is replaced by a mixture density at the inlet.

$$H = \frac{\frac{\sum_{i=1}^{8} p_{t,MPP_i}}{8} - p_{t,MPS}}{g(\alpha_l \rho_l + \alpha_g \rho_g)} \qquad (6)$$

The blade pressure at any radii $p_{Bl,i}$ is determined by equation (7). In this equation $p_{s,bl,i}$ is the pressure at radial position i and p_{MPS} the pressure at inlet.

$$p_{Bl,i} = p_{s,bl,i} - p_{s,MPS} \qquad (7)$$

Single-phase flow

In figure 4 the single-phase flow performance curves (H, P_i, η_i) are shown for the experiment and the full geometry, steady simulation model at three rotational speeds.
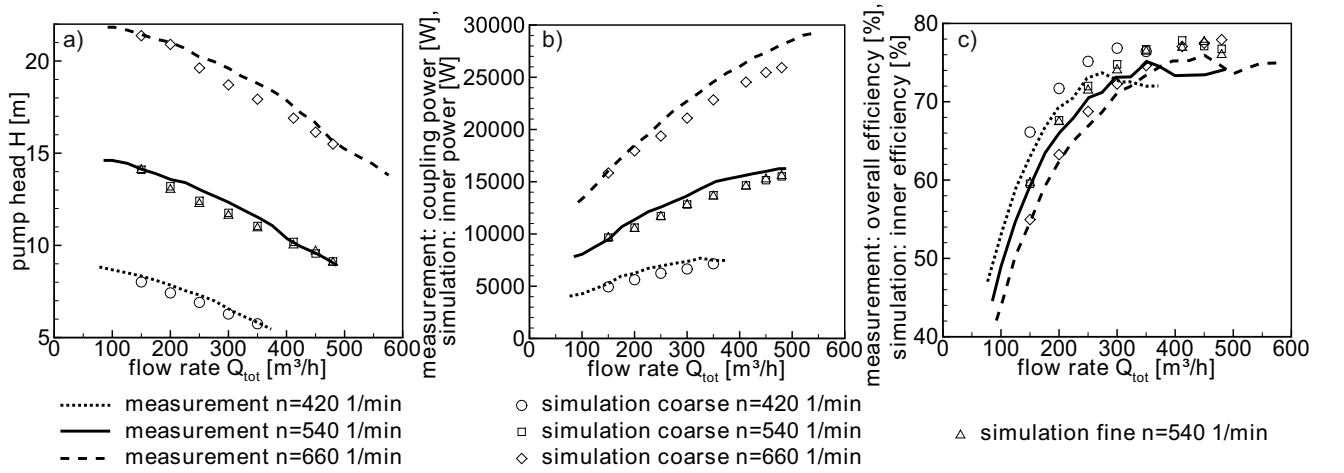
Figure 4: **Single-phase flow performance curves of the full model for diff. speeds**

The head is well predicted: The maximum head deviation between simulation and experiment is smaller than $0.5\ m$ for all operation points. The inner power curve from the simulation is compared to the measured coupling power. The coupling power is underestimated by the simulation. As the evaluation of the inner power does not consider the mechanical losses, the observed tendency of increasing underestimation with a rising rotational speed is feasible. Thus, the efficiency is overestimated by the simulation, while the trend of increasing efficiency with decreasing speed up to a flow rate of $300\ m^3/h$ is well captured.

It can be concluded that the full steady model is sufficiently accurate to reflect the trends of the performance curves. Possible remaining sources of inaccuracy are the turbulence model, slight geometry simplifications as well as the neglect of transient effects.

For a rotational speed of $n = 540\ 1/min$, the single channel model results are compared to the full model results and the data, cf. fig. 5 a. The single channel results show a slightly higher head than the full model, consistent with the neglect of the side chamber flow. Somewhat uncommon is the observation that the difference between single channel and full model head is very small at low flow rate, since usually for decreasing flow rate an increasing influence of side chamber secondary flow can be expected in radial pumps. In fact, the gap flow rate shows a local maximum at $300\ m^3/h$ and decreases for low flow rates, cf. fig. 5 b. The small influence of the side chambers is attributed to the uncommon characteristics of the research pump, in particular to the low head.
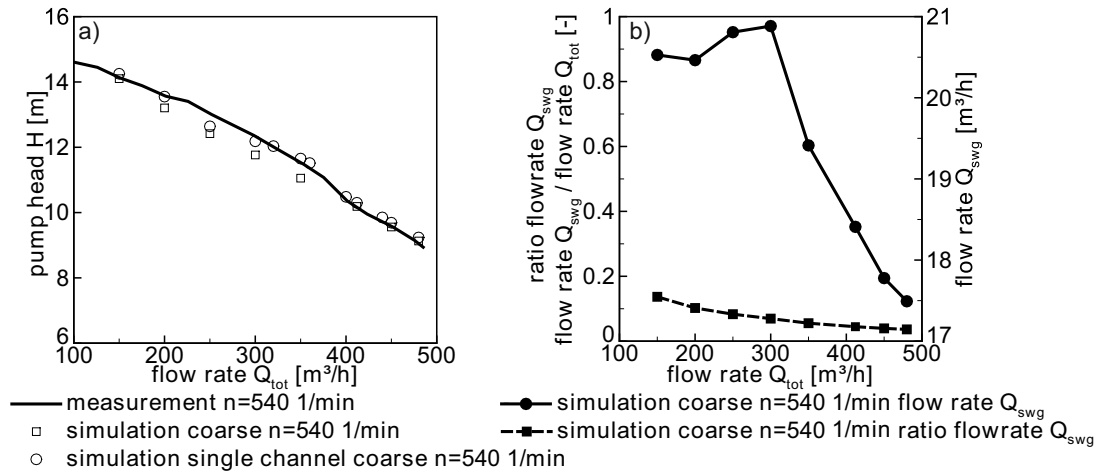
Figure 5: **Single-phase flow pump head curve for n = 540 1/min of both, the single channel and the full model (a) and side wall gap flow rate of full model (b)**

Summarizing, the deviation of the predicted head between full and single channel model is in the same order of magnitude as the deviation of the full model results to the measurement data. It can be assumed that it is sufficient to utilize the single channel model for the subsequent two-phase simulations, which is to be verified in the future by comparing the results of the two-phase flow simulations with both, full and single channel model.

Two-phase flow

In fig. 6 a the measured head curves in dependence on the flow rate are depicted for different IGVF. A drop of head can be observed with increasing IGVF, which is most distinctive for IGVF between 3 % and 5 %. The corresponding single channel simulation results are depicted in fig. 6 b and show qualitatively the same tendency as the measurement up to IGVF of 3 %. The maximum head deviation between experiment and simulation is smaller than 2 m at a flow rate of 480 m^3/h and a IGVF of 3 %.
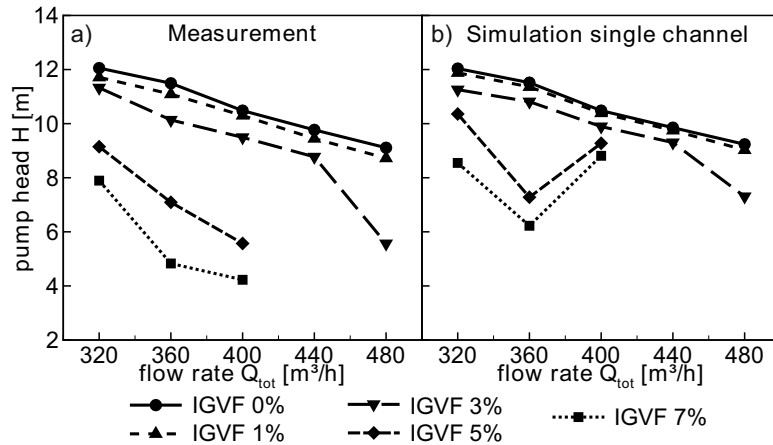

Figure 6: **Calculated pump head curves for multiple IGVF compared to experimental data**

For higher IGVF, i.e. 5 % and 7 %, a qualitatively different trend than observed in the measurements is discernible in the simulation results: the predicted head curve rises sharply by increasing the flow rate from 360 m^3/h to 400 m^3/h, while the head curve continues decreasing in the experiment. To figure out the source of the basically different result in the simulation, the predicted blade pressure profiles midway between hub and shroud are compared to the experimental data (Suryawijaya and Kosyna, 2000) for the flow rates of 360 m^3/h and 400 m^3/h exemplary for the IGVF of 3 % and 5 %

8

in figure 7. Regarding the measurement, only minor differences in the pressure profiles between flow rates of 360 m^3/h and 400 m^3/h are discernible, cf. fig. 7 a and c. By a rise of the IGVF from 3 % to 5 %, the pressure side pressure level collapses in the vicinity of the leading edge and only recovers partly further downstream. It can be assumed that in the experiment a large bubble is present at the pressure side in leading edge vicinity. This assumption is supported by the flow visualisations by Wunderlich (1981, 2014).
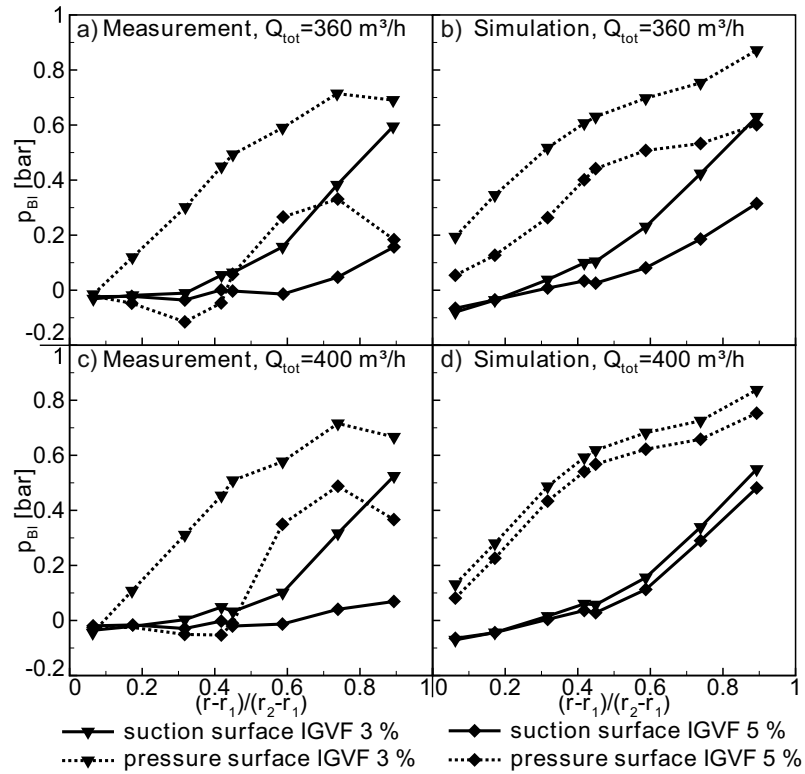
Figure 7: **Calculated two-phase flow blade pressure profiles compared to experimental data at mid span**

In the simulation at a flow rate of 360 m^3/h, cf. fig. 7 b, a significant drop of the pressure profile can be observed on both, the pressure and the suction side. While the drop at the suction side is similar to the pressure drop in the experiment, on the pressure side, the collapse of pressure close to the leading edge cannot be observed but a rather uniform pressure decrease along the pressure side blade profile is present. For increased flow rate, 400 m^3/h, the drop of the pressure profile on both, the pressure and the suction side, is less distinction than for 360 m^3/h. As a consequence, the head increases with increasing flow rate from 360 m^3/h to 400 m^3/h at IGVF > 3 %, cf. fig. 6 b. The head increase (cf. fig. 6 b) at IGVF > 3 % for increasing flow rate and the corresponding change in pressure profile, cf. fig. 7 b and d, can be attributed to the flow pattern, in particular the region where gas accumulates within the blade channel.

Exemplary contour plots of arbitrary time instances of the GVF for operation points 360 m^3/h and 400 m^3/h and for the IGVF of 3 % and 5 % are shown in figure 8. For a IGVF of 3 % at a flow rate of 360 m^3/h, cf. fig. 8 a, gas accumulates close to the suction surface and the trailing edge, whereas for a flow rate of 400 m^3/h cf. fig. 8 b, the bubbles accumulate rather in the center of the blade channel. By increasing the IGVF to 5 % for a flow rate of 360 m^3/h cf. fig. 8 c, the size of the gas accumulation region as well as the GVF increase considerably, while for a flow rate of 400 m^3/h, cf. fig. 8 d, they increase only moderately. An accumulation close to the pressure side and the leading edge as observed in the measurements even for very low values of IGVF is not discernible.

However, a small gas accumulation region can be observed (not shown here) for higher IGVF, i.e. 7 %, at the pressure side close to the leading edge, but for lower IGVF than 7 % it is not present in the simulation results.
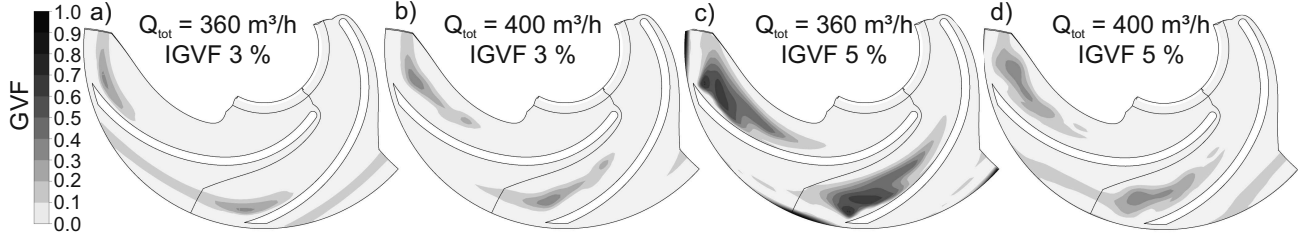

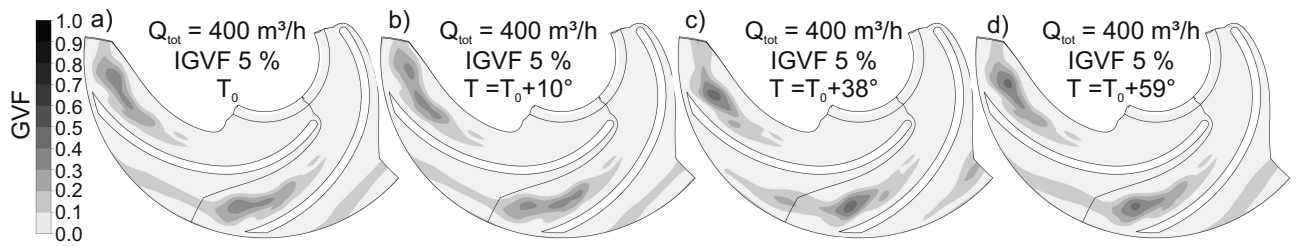Figure 8: **GVF in blade channel at mid span for two operations points and two IGVF**

Figure 9: **GVF in blade channel at mid span for 400 m^3/h and 5 % IGVF at diff. timesteps**

The source of the lower gas region size and lower GVF for 400 m^3/h, cf. fig. 8 d, is the convection of gas out of the blade channel for this higher flow rate in a highly unsteady way, while the flow field is essentially steady for the lower flow rate, 360 m^3/h. To illustrate the unsteady nature of the flow for 400 m^3/h, a time sequence of contour plots of the GVF is presented in figure 9. The gas accumulates within the blade channel in a certain distance of the blade walls, cf. fig. 9 a. After growing to a higher level of GVF, the gas accumulation region divides into two parts, cf. fig. 9 b. The downstream part of gas is convected out of the blade channel, cf. fig. 9 c. Then, this process starts again, fig. 9 d and repeats periodically. The duration of one period corresponds to a time of about 59° rotor rotation.

CONCLUSIONS

In this paper it is evaluated if the head drop with increasing IGVF in a radial pump is captured by a state of the art CFD code with a mono-disperse phase model. The qualitative trend of the head vs. flow rate is well captured at IGVF up to 3 %. For higher IGVF, even no qualitative agreement between measurement and simulation results can be achieved, cf. fig. 6: for IGVF > 3 % and for increasing flow rate from 360 to 400 m^3/h, the simulation predicts a rise in head in contrast to the experimental data. The experimentally obtained pressure profiles by Suryawijaya and Kosyna (2000), supported by visualization by Wunderlich (1981, 2014) imply that there are gas accumulations at the blade surface, in particular at the pressure side close to the leading edge that lead to a drop of the pressure, discernible in fig. 7. In the simulation, however, the gas accumulations occur rather in the center of the channel and neither at the blade wall nor in the vicinity of the leading edge.

As a consequence, at low flow rates, a rather smooth pressure side drop of the pressure can be observed. With increased flow rate, the gas regions within the channel are convected downstream in an unsteady way, so that the blade pressure decrease is more moderate than for smaller flow rates and the head rises. This observation is in significant contrast to the experimental finding.

Different reasons for the accumulation of gas at the wrong location are assumed, namely the channel center far away from the blade walls. First, the simplification of the single channel model is to be verified and the mesh sensibility analysis has to be done also for multi-phase flow. Secondly, lift

forces are neglected in this first attempt to predict the liquid-gas characteristics of radial pumps. However lift forces will play a significant role for the deflection of gas bubbles toward the blade wall. In addition, bubbles are deflected in dependence on their size. Not only the magnitude, but even the direction of deflection may depend on the bubble size, cf. Krepper et al. (2007). This present approach (mono-dispersed model) cannot account for this effect. Therefore, the multi-phase model should be extended by a poly-dispersed phase model in combination with bubble interaction, i.e. break-up and coalescence models. These possible sources of mis-location of the gas accumulation region in the simulation are the subject of further research of the authors.

ACKNOWLEDGEMENTS

REFERENCES

Ansys Inc. (2014): *Ansys CFX-Solver Theory Guide*, Release 15.0., Ansys Inc., Canonsburg, PA USA

Cappelino, C.A., Roll, D.R., Wilson, G. (1992): *Design Considerations and Application Guidelines for pumping Liquids with Entrained Gas using open Impeller Centrifugal Pump*, Int. Pump User Symposium, Vol. 9, pp. 51-60

Caridad, J., Asuaje, M., Kenyery, F., Tremante, A., Aguillon, O. (2008): *Characterization of a centrifugal pump impeller under two-phase flow conditions*, Journal of Petroleum Sci. and Eng., Vol. 63, pp. 18-22

Furukawa, A., Togoe, T., Sato, S., Takamatsu, Y. (1988): *Fundamental Studies on a Tandem Bladed Impeller of Gas/Liquid Two-Phase Flow Centrifugal Pump*, Memoirs of the Faculty of Engineering Kyushu University, Vol. 48, No. 4, pp. 231-240

Gülich, J.F. (2010): *Kreiselpumpen: Handbuch für Entwicklung, Anlagenplanung und Betrieb*, Berlin, Heidelberg, New York, Springer

Hlawitschka, M. W., Chen, F., Bart, H.-J., Hagen, H. (2011): *CFD Simulation und verbesserte Datenauswertung einer Extraktionskolonne vom Typ Kühni*, Young Researchers Symposium, Nachwuchsring des Landesforschungszentrum Center for Mathematical and Computational Modelling (CM^2), University Kaiserslautern

Krepper, E., Frank, T., Lucas, S., Prasser, H.-M., Zwart, P.J. (2007): *Inhomogeneous MUSIG model – a population balance approach for poly-dispersed bubbly flow*, 12. Int. Topic Meeting on Nuclear Reactor Thermal Hydraulics (NURETH-12)

Minemura, K., Murakami, M. (1980): *A Theoretical Study on Air Bubble Motion in a Centrifugal Pump Impeller*, Proc. ASME/JSME Fluid Eng. Conf., Fed-Vol. 102, pp. 446-455

Minemura, K., Murakami, M., Katagiri, H. (1985): *Characteristics of Centrifugal Pump Handling Air-Water Mixtures and Size of Air Bubbles in Pump Impellers*, Bulletin of the JSME, Vol. 28, No. 244, pp. 2310-2318

Minemura, K., Uchiyama, T. (1993a): *Prediction of Pump Performance Under Air-Water Two-Phase Flow Based on a Bubbly Flow Model*, Trans. American Soc. of Mech. Eng., Vol. 115, No. 4, pp. 781-783

Minemura, K., Uchiyama, T. (1993b): *Three-Dimensional Calculation of Air-Water Two-Phase Flow in Centrifugal Pump Impeller Based on a Bubbly Flow Model*, Trans. American Soc. of Mech. Eng., Vol. 115, No.4, pp. 766-771

Murakami, M., Minemura, K., Suehiro, H. (1971): *Effects of Entrained Air on the Performance of Centrifugal and Axial Flow Pumps*, Memoirs of the Faculty of Engineering of Nagoya University, 23-1, pp. 124-133

Pak, E.T., Lee, J.C. (1998): *Performance and pressure distribution changes in a centrifugal pump under two-phase flow*, Proc. of the Inst. of Mech. Engineers, Part A, Vol. 212, No. 3, pp. 165-171

Sato, S., Furukawa, A., Takamatsu, Y. (1996): *Air-water two-phase flow performance of centrifugal pump impellers with various blade angles*, JSME Int. Journal Japanese Soc. Mec. Eng., Series B, Vol. 39, No. 2, pp. 223-229

Schiller, L., Naumann, A. (1933): *Über die grundlegenden Berechnungen bei Schwerkraftaufbereitung*, Zeitschrift des Vereines deutscher Ingenieure, Vol. 77, Nr. 12

Suryawijaya, P., Kosyna, G. (2000): *Schaufeldruckmessungen im rotierenden System an einer Radialpumpe bei Gas/Flüssigkeitsgemischförderung*, Chemie Ing. Technik, Vol. 72, pp. 1366-1371

Tillack, P. (1998): *Förderverhalten von Kreiselpumpen bei viskosem, gasbeladenem Fördermedium*, Ph.D. thesis, Tecnical University Kaiserslautern

Wan, Y. P. and Peters, N. (1999): *Scaling of Spray Penetration with Evaporation*, Atomization and Sprays 9, pp.111-132

Wulff, D. (2014): *personal communication*, Institute of Jet Propulsion and Turbomachinery, Tecnical University Braunschweig

Wunderlich, B. (1981): *Experimentelle Untersuchung zum Förderverhalten von Kreiselpumpen bei Flüssig-keits-Gasgemischen*, Ph.D. thesis, University Magdeburg

Wunderlich, B. (2014): *personal communication*, Institute of Fluid Dynamics and Thermodynamics, University Magdeburg

Yu, Z.Y., Zhang, Q.Z., Huan, R., Cao, S.L. (2012): *Numerical analysis of gas-liquid mixed transport process in a multiphase rotodynamic pump*, IOP Conf. Series: Earth Environ. Sci., Vol. 15